

Recent Results from the AMANDA-II neutrino telescope

Andreas Groß for the AMANDA collaboration
Institute of Physics, University of Dortmund, 44221 Dortmund



AMANDA-II is an operating neutrino telescope located at the South Pole. Recent results of AMANDA are presented, including the examination of the diffuse neutrino flux, permanent and transient point source analyses, and indirect dark matter searches. A brief outlook on the IceCube neutrino telescope currently under construction at the South Pole is given.

1 Introduction

The observation of high-energy cosmic rays - both charged particles and photons - motivates the search for extraterrestrial high-energy neutrinos. Charged particles have been detected up to energies around 10^{20} eV while photons up to tens of TeV could be attributed to point sources. Most of the production mechanisms of highly energetic nuclei as well as hadronic models for the TeV γ radiation imply the coproduction of high-energy neutrinos. This allows neutrinos to be used as astrophysical messengers giving additional information on the production mechanisms in different astrophysical environments. Due to their small cross section and their lack of an electrical charge, ν 's do neither suffer from deflection nor absorption on the way from the source to the Earth. This small cross section, however, requires very large detector volumes in order to provide the observer with sufficiently high ν induced event rates.

2 The AMANDA neutrino telescope

The AMANDA neutrino telescope at the geographic south pole was built in the years 1995-2000 in the antarctic ice sheet. AMANDA-II consists of 677 optical modules (OMs) containing photomultiplier tubes (PMTs) on 19 strings in the south pole ice^a. The geometrical shape of the detector is a cylinder with a diameter of 200 m. Most modules are concentrated at depths between 1500 m-2000 m.

^aThe AMANDA-B10 subdetector was running from 1997-1999 with 302 OMs on the inner 10 strings.

Most of the events triggered by AMANDA are atmospheric muons reaching the detector from above. Muons produced in charged current (CC) interactions of ν_μ can be separated from atmospheric ones by taking into account directional and energy information.

The Earth serves as a shield against any other particles, such that upgoing muons must be ν_μ induced. The lower AMANDA threshold for ν_μ -induced events is around 50 GeV, while at PeV energies, the Earth becomes opaque for ν_μ . Thus, for energies below a few PeV, AMANDA's field of view for ν_μ is restricted to the northern sky. At higher energies, the search for downgoing ν_μ induced events is possible since the background of atmospheric muons falls steeply with energy. Muons travel long distances through the ice emitting continuously Cherenkov light. This increases the effective volume of the detector and provides a long lever arm for track reconstruction. An angular resolution of 3° and below has been achieved, depending on the declination angle and on the strength of quality cuts. Other ν flavors can be detected by the light produced by hadronic and electromagnetic cascades, if the interaction takes place within the detector. In the cascade channel, energy resolution is much better, but the event rates are lower. Due to the lack of a long lever arm, the angular resolution is only about 30° . Here, we focus on the ν_μ channel and energies below 1 PeV.

3 Cosmic accelerators

The existence of highly energetic cosmic rays can be explained by the mechanism of Fermi acceleration. Statistically, a charged particle gains energy passing an electromagnetic shock front. The random energy gain results in a power law spectrum for the cosmic ray flux with a spectral index $\gamma \approx 2$. A review on cosmic ray production by shock acceleration can be found in ¹.

The accelerated protons interact with each other or ambient photons. Thus, charged and neutral pions are produced mostly via the Δ resonance. Pion decay yields a ν flux with roughly the same spectral index as the protons. At production site, the ν flavors are distributed according to $\nu_e : \nu_\mu : \nu_\tau \approx 1 : 2 : 0$. Due to ν oscillations, an approximate equipartition of flavors is predicted to be observed at the detector.

The extremely high total energy needed for particle acceleration to ultra-high energies (UHE) energies suggests the gravitational potential of a black hole or a neutron star as the source. Likely astrophysical environments for shock acceleration are jet-disc systems like Active Galactic Nuclei (AGN), Gamma Ray Bursts (GRBs) and Microquasars as well as shock fronts from Supernova explosions expanding into the interstellar medium or into the wind of the preceding star.

Additional to the described shock acceleration mechanism, top-down scenarios for the production of cosmic rays are discussed. These models assume the decay of heavy non-Standard Model (SM) particles (see e.g. ²).

4 Physics analysis strategies

After selecting upgoing muon tracks with high quality reconstruction fits, the resulting AMANDA event samples are strongly dominated by atmospheric ν_μ . Several analysis strategies have been developed to analyze these atmospheric ν_μ and to search for astrophysical ν_μ . In the diffuse analysis, extraterrestrial ν_μ can be detected by a significant excess of the number of highly energetic ν_μ over the expectation from the atmospheric ν_μ flux. In point source analyses, the directional information is used to search for an excess of ν_μ coming from the direction of a potential source. For time-dependent sources like GRBs, the arrival time information can be used for a further background reduction.

The AMANDA collaboration follows a strict blindness policy, i.e. an analysis has to be developed blindly with respect to the data. That ensures a statistical correct analysis. In

practice, that means that all optimizations are done on a subsample of data that is not used for the final result or that the relevant quantities are randomized (e.g. reconstructed right ascension in a point source analysis).

5 Diffuse neutrino spectrum

The energy losses of muons in the ice consist of an almost energy independent part by due to ionization and energy-dependent stochastic losses due to radiative processes. The energy loss is parameterized as $dE/dx = a + bE$, where $a/b \approx 600$ GeV. Thus the amount of Cherenkov light deposited turns out to be proportional to the energy and allows for energy reconstruction.

With help of a full Monte Carlo simulation chain, some energy dependent variables were identified, e.g. the number of hit OMs. A neural net was trained with a high number of MC events using 6 input variables and detector settings of the year 2000. For each measured event an energy correlated parameter is determined by the neural net. In order to correct for the limited acceptance and for the finite resolution of the detector, the method of regularized unfolding is used⁶. The correction for the energy losses at the vertex is also done within the unfolding. With the input of the energy correlated parameter from the neural net and two further energy dependent variables for all events, the measured ν_μ spectrum is determined.

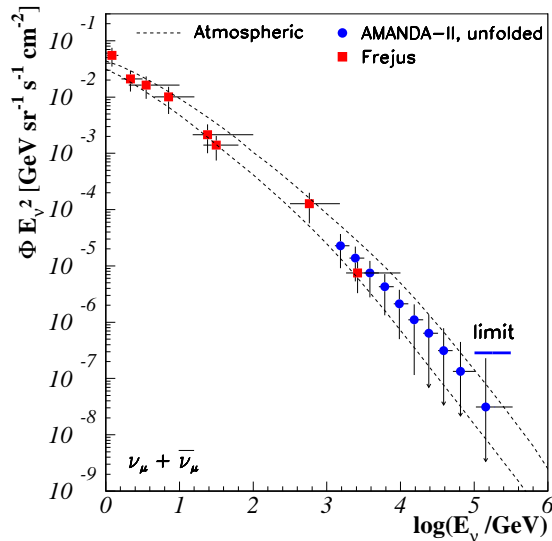


Figure 1: Unfolded neutrino ($\nu_\mu + \bar{\nu}_\mu$) energy spectrum as measured by AMANDA II and Frejus. The AMANDA II limit on the E^{-2} flux is marked by the solid line above the highest energy bin.

The preliminary unfolded ν_μ spectrum of AMANDA II based on events from the year 2000 is displayed in Fig. 1 together with lower energy measurements of Frejus³. All data points are in agreement with the expectation for the atmospheric ν_μ flux. For energies above 100 GeV, the expectation is taken from the prediction in⁴, for lower energies the parametrization from⁵ is used. The prediction for the horizontal flux is given by the upper line, while the lower line corresponds to the expectation for the vertical flux.

The unfolded spectrum provides one possibility to calculate a limit on an additional E^{-2} flux. The highest energy bin at 100 TeV-300 TeV was determined to be most sensitive to the additional contribution. Since the statistics of the unfolding output is unknown a priori, the probability density function (pdf) of the results from the unfolding program has to be determined with Monte Carlo simulations. For various signal contributions between $10^{-8} \text{GeV s}^{-1} \text{cm}^{-2} \text{sr}^{-1}$ and

$10^{-6}\text{GeV s}^{-1}\text{cm}^{-2}\text{sr}^{-1}$, large numbers of MC experiments are performed. The pdf is extracted from histograms of the output of the unfolding program for the MC experiments. With the pdf, Feldman-Cousins confidence belts⁷ are constructed. By using these confidence belts, the 90% C.L. upper limit for the year 2000 data is determined preliminarily to

$$E^2\Phi < 2.6 \cdot 10^{-7}\text{GeV s}^{-1}\text{cm}^{-2}\text{sr}^{-1},$$

including 33% for systematical uncertainties (mainly due to unknown ice parameters).

6 Point source analysis

In addition to diffuse analyses, the directional information of ν_μ events can be used in a point source analysis to identify individual ν sources. From the data collected in the years 2000-2003 (livetime 807 days), an event sample was extracted for point source analyses containing 3329 upgoing tracks. Quality cuts on the fitted tracks ensure a good angular resolution and a minimal contamination by misreconstructed atmospheric muons. The event selection was optimized for best sensitivity to point sources with spectral indices γ between $\gamma = -3$ and $\gamma = -2$. The event sample was searched for a significant excess of ν_μ from a point source.

6.1 Steady point sources

Since ν production via pion decay implies the co-production of high energetic γ radiation, strong γ sources are good candidates for highly energetic ν emission. Thus, a list of 33 pre-selected source candidates, mainly consisting of high energy γ sources, was analyzed. The candidate list covers 13 blazars, 3 nearby AGN and galactic source candidates such as microquasars and supernova remnants. For none of the 33 selected sources, a significant signal was found. The highest excess was found for the Crab nebula with 10 events at a background of 5.36 events. The background probability is given by $\log P = -1.35$. Considering the trial factors, such an excess is expected for one of the 33 sources with 64% probability in a pure background sample.

Additionally, in an all-sky search, ν point sources at any point of the sky have been searched by a grid of overlapping bins. These bins were tested for a significant excess over the background expectation determined by the number of events coming from the same zenith band. The highest significance in any bin (before correction for the trial factor) was found with 3.35σ . A toy MC shows that this value can be expected with a probability of 92% in a random sample.

Furthermore, an unbinned method was used, calculating the significance for an excess over the background given the track direction and the resolution of the individual reconstructed events, as determined from the fit uncertainties⁹. The significance sky map from this method, as displayed in Fig. 2, shows no deviation from a sky map of the same sample with randomized right ascension.

Hence, no statistically significant excess was found from any steady point source. On all source candidates, upper limits were calculated. The preliminary results presented here update the published results for data collected in 2000-2002⁸.

6.2 Source stacking of AGN

In order to increase the sensitivity of telescopes, so called source stacking methods have been applied in γ astronomy and in optical astronomy. In a source stacking analysis, the cumulative signal of several sources of the same type is evaluated. A systematical classification is required to define the relevant source samples.

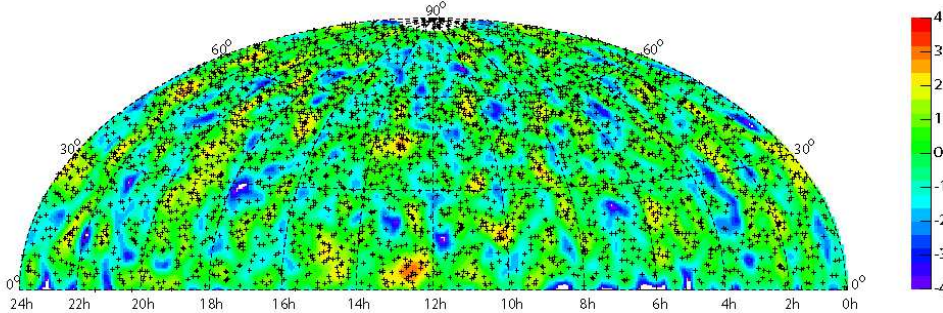


Figure 2: Significance sky map of the point source analysis (preliminary). The dots correspond to the reconstructed arrival directions of individual events.

For AMANDA, a source stacking analysis of AGN has been developed based on a phenomenological classification. The axisymmetry of AGN is one central ordering parameter yielding different appearance of AGN depending on the observer’s angle to the AGN axis. If this angle is small, an AGN appears as a blazar and emission from the jet gets boosted. A further difference is the strength of the radio flux of the AGN, resulting in a classification into radio-loud AGN and radio-weak ones.

The ν production mechanism via Δ resonance and pion decay implies correlations between the photon spectrum and the ν spectrum at the production site. These correlations may be distorted, if sources are optically thick for photons. In case of optically thick sources, the high energy photons induce electromagnetic cascades. Then photon energies get reprocessed and the photon flux is shifted to lower energies. Taking into account the high cross sections of photons, the current knowledge about AGN does not exclude optical thickness effects for high energy photons in AGN.

The possibility of optical thickness motivates a selection also at lower γ energies than the AMANDA threshold for ν . In total, 11 samples were compiled. The number of sources to be included in the source stacking analysis is optimized with the hypothesis that the relative TeV ν flux of sources is proportional to the relative photon flux at selection energy. For details of the source selection see¹⁰.

An application of the stacking method with the year 2000 data on these source classes showed no significant excess over the background expectation. We calculated 90% C.L. upper limits on the integral flux of ν_μ above 10 GeV of $(0.1 - 1.3) \cdot 10^{-8} \text{cm}^{-2}\text{s}^{-1}$ per source. This is significantly smaller than the sensitivity^b of $2 \cdot 10^{-8} \text{cm}^{-2}\text{s}^{-1}$ of the point source analysis for individual sources of that sample.

6.3 Time-variable studies of preselected sources

Additionally to the searches for steady point sources, a search for a time-variable signal has been done. In this search, several candidate sources which are known to be highly variable were analyzed. Two different search strategies have been used:

- *Search for clusters of events in coincidence with identified periods of enhanced photon emission - Multiwavelength approach:* Three objects have been analyzed, two blazars (Mkn 421 and 1ES 1959+650) and a microquasar (Cyg X-3). The active periods have been defined by the X-ray light curves for the blazars and by the radio light curve for the microquasar.
- *Search for occasional ν bursts:* A catalogue of 12 highly variable source candidates was investigated. No assumption on the time of the occurrence of ν flares is made a priori.

^baverage 90% C.L. upper limit on flux in case of absence of signal

A sliding time window of fixed duration is searched for excesses of events. The duration of the time window is set to 20 days for galactic sources and to 40 days for extragalactic ones. Monte Carlo simulations of various scenarios of flare duration support this choice of the duration.

The searches have been performed following the AMANDA blindness principle such that biases which cannot be quantified are avoided. As a preliminary result, in both approaches, no significant excess has been found for any of the sources analyzed. In the multiwavelength approach, the highest excess was found for 1ES 1959+650 with 2 events on a background of 1.57 events. In the search for occasional ν bursts, for GRS 1915+105 and for 1ES 1959+650 doublets have been found with background probabilities of 32% and 34%, respectively.

In an a-posteriori analysis of the 1ES 1959+650, the arrival times of the individual ν 's were considered. One of the events is within a few hours from a reported flux peak in the Whipple light curve¹¹. Since X-ray measurements do not show a peak, this peak is considered as an "orphan flare". An "orphan flare" is a flare in the high energy gamma-ray range (TeV) without a coincident increase in X-ray (keV) emission. As active periods are selected on the basis of the X-ray light curves, this event is not present in the preselected active periods. Exceptions from the usually observed correlations between keV and TeV fluxes are seen as an indication of hadronic mechanisms responsible for TeV emission.

Even though the theoretical background draws attention to this observation, it must be stressed that the probability of a random coincidence of the AMANDA event with the time of the flare is difficult to evaluate. Additionally, in all reasonable scenarios, a significant detection at a 5σ level can be excluded.

7 Gamma Ray Bursts

Gamma Ray Bursts (GRBs) are transient phenomena emitting a very high amount of γ radiation in a very short time. Under the assumption of isotropic radiation, their luminosity reaches 10^{51} erg/s. Typical burst durations vary between 0.1 s and 1000 s. While their nature remained unknown for a long time, the fireball model recently turned out to describe the phenomenology successfully. According to the fireball picture, GRBs are formed by the collapse of a massive precursor object. Similar to AGN, the collapse is not rotational symmetric and the conservation of angular momentum results in the occurrence of two jets along the rotation axis. In these jets, shock waves propagate and when reaching the surface, they emit the observed γ radiation. The beaming effects reduce the necessary energy supply of the GRB. A connection of GRBs to supernovae of type Ic is confirmed by observations of GRB030329 and GRB/980425. The diffuse energy spectrum of ν from GRBs has been predicted by the assumption that ν and γ are produced by the same hadronic mechanism¹². This results in the broken power law spectrum, which we will refer to as the Waxman-Bahcall (WB) spectrum.

The location in space *and* in time allows to search with AMANDA for ν from GRBs at a very low background. An analysis of 139 bursts in the years 2000-2003 was optimized for the WB spectrum. The time interval was chosen to cover 90% of the photon signal. For none of the bursts, an event was found in that time window. The total background expectation is 1.25 events. From that result, a preliminary 90% C.L. upper limit on the WB spectrum of $E^2\Phi < 3 \cdot 10^{-8} \text{GeV cm}^{-2}\text{s}^{-1}$ was calculated.

The possibility of ν leaving the source while it still remains optically thick for γ is taken into account by a precursor analysis, covering the time before the measured burst. Again, no signal was found. In the future, an optimization of the analysis for individual burst parameters can increase the sensitivity.

8 Indirect WIMP searches

The minimal supersymmetric extension of the standard model (MSSM) provides a promising dark matter candidate, the lightest neutralino $\tilde{\chi}_0^1$, a linear combination of the supersymmetric partners of the electroweak neutral gauge and Higgs bosons. Assuming R-parity conservation, the $\tilde{\chi}_0^1$ is stable. according to this scenario, trapping in the gravitational potential of the Sun or the Earth may increase the neutralino density there. Then, pairwise annihilation gets enhanced and the decay of the annihilation products yields a high energy neutrino flux. A high energy neutrino flux from these regions can only be interpreted as the annihilation of non-SM particles, since the solar neutrino flux from the standard model is restricted to MeV energies.

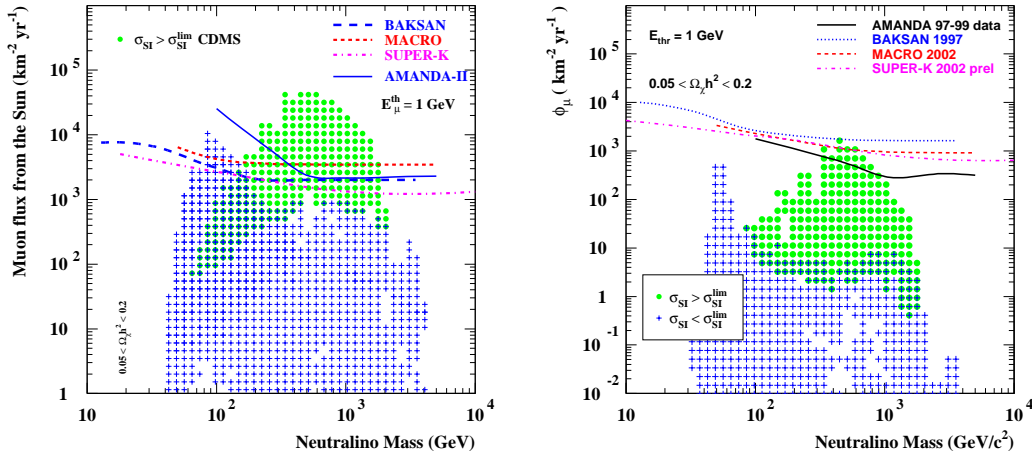


Figure 3: Limits on muon flux from WIMPs annihilating in the Sun (left) or in the Earth (right).

The sensitivity of AMANDA towards SUSY dark matter has been investigated by Monte Carlo simulations with the program DARKSUSY¹³. For different neutralino masses between 50 GeV and 5 TeV, two annihilation channels were considered: The soft channel $\tilde{\chi}_0^1 \tilde{\chi}_0^1 \rightarrow b\bar{b}$ and the hard channel $\tilde{\chi}_0^1 \tilde{\chi}_0^1 \rightarrow W^+W^-$. The terms soft and hard refer to the fraction of total energy being emitted in ν .

The size of the search bin was optimized for the expected neutrino spectrum for the different channels and neutralino masses. For solar WIMPs and data collected in 2001, the optimal bin size varies between 5.5° for the hardest spectrum and 26° for the softest spectrum. In this analysis, no significant excess over the atmospheric background was found. The resulting limits on the integrated muon flux for the hard channel are plotted in Fig. 3 on the left hand side. Limits from other indirect searches e.g. from SUPER-K are also plotted. In that plot, the points represent the expectation for different SUSY parameters. The expectations are calculated with DARKSUSY. Values disfavored by the direct search for WIMPs in CDMS II¹⁴ marked by darker points. The restrictions on the parameter space due to the direct search appear more severe. However, it should be noted the two methods are complementary. They probe the WIMP distribution in the solar system at different epochs and they are sensitive to different parts of the velocity distribution. A detailed discussion of the results of the solar WIMP analysis with AMANDA can be found in¹⁵.

For WIMPs from the Earth, data collected with the AMANDA-B10 subdetector in 1997-1999 (livetime 433 days) was analyzed with the same method. No significant excess over the background expectation was found. In the same way as for solar WIMPs, the resulting preliminary limits of that analysis are displayed in Fig. 3 on the right hand side.

9 Conclusions and outlook

The AMANDA-II neutrino telescope has been operating successfully since 2000 and yielded remarkable results. AMANDA has measured the atmospheric ν_μ flux up to 100 TeV. No extraterrestrial ν flux has been detected so far. The upper limits on the flux, as set in the different analyses, already constrain various theoretical models.

While the analysis of AMANDA data goes on, in January 2005, the construction of the IceCube neutrino telescope¹⁶ began with the successful deployment of the first string with 60 digital OMs (DOMs). In the final stage, IceCube will reach a cubic kilometer size instrumented with 4800 DOMs on 80 strings. The surface array IceTop will have stations near the top of each string. Each station will consist of 2 tanks of frozen water viewed by standard IceCube DOMs. IceTop will allow for coincident surface and in ice measurements of air showers induced by cosmic rays.

The existing AMANDA strings will be integrated in IceCube as a more densely instrumented detector region. The increase in sensitivity with IceCube is considered to be sufficient for the detection of astrophysical ν fluxes in most theoretical models.

Acknowledgments

We acknowledge the support from the following agencies: The U.S. National Science Foundation, the University of Wisconsin Alumni Research Foundation, the U.S. DoE, the U.S. NERS Computing Center, the UCI AENEAS Supercomputer Facility, the Swedish Research Council, the Swedish Polar Research Secretariat, the Knut and Alice Wallenberg Foundation (Sweden), the German Federal Ministry of Education and Research, the Deutsche Forschungsgemeinschaft, the IWT (Belgium), the FWO (Belgium), the FNRS (Belgium) and the OSTC (Belgium). D. F. Cowen acknowledges the support of the NSF CAREER program.

1. R. J. Protheroe, In: Towards the millenium in Astrophysics, Problems and Prospects. International School of Cosmic Ray Astrophysics 10th Course. p. 3. (1998).
2. M. Drees, hep-ph/0310331.
3. K. Daum et al. (Frejus collaboration) Zeitschrift für Physik C66 (1995) 177.
4. L. V. Volkova and G. T. Zatsepin, Soviet Journal of Nuclear Physics 37 (1980) 212.
5. M. Honda et al., Phys. Rev. D52 (1995) 4985
6. V. Blobel, Technical Note TN 361, OPAL (1996).
7. G. J. Feldman, R. D. Cousins, Phys.Rev. D57 (1998) 3873-3889.
8. M. Ackermann et al. (AMANDA collaboration), Phys.Rev. D71 (2005) 077102.
9. T. Neunhoffer, astro-ph/0403367 (2004).
10. M. Ackermann et al. (AMANDA collaboration), in prep.
11. D. Holder et al., ApJ 583, L9 (2003).
12. E. Waxman and J. Bahcall, Phys.Rev.Lett. 78 (1997) 2292.
13. P. Gondolo et al., Journ. of Cosmol. & Astropart. Phys. 0407 (2004) 0008.
14. D. S. Akerib et al., Phys.Rev.Lett. 93 (2004) 211301.
15. M. Ackermann et al. (AMANDA collaboration), to be published.
16. J. Ahrens et al. (IceCube collaboration), Astropart. Phys. 20 (2004) 507.